Plant Physiology and Biochemistry 134 (2019) 113–122

Contents lists available at ScienceDirect

Plant Physiology and Biochemistry

journal homepage: www.elsevier.com/locate/plaphy

Research article

Transcriptional profiling and physiological analysis reveal the critical roles of ROS-scavenging system in the Antarctic moss *Pohlia nutans* under Ultraviolet-B radiation☆

Chengcheng Li[a,1], Shenghao Liu[b,1], Wei Zhang[c], Kaoshan Chen[a], Pengying Zhang[a,*]

[a] National Glycoengineering Research Center, School of Life Sciences, Shandong University, Jinan, 250100, China
[b] Key Laboratory of Marine Bioactive Substance, The First Institute of Oceanography, State Oceanic Administration, Qingdao, 266061, China
[c] School of Environment, Qingdao University, Qingdao, 266061, China

ARTICLE INFO

Keywords:
Antarctic moss
Differentially expressed genes (DEGs)
Flavonoids
Ultraviolet-B radiation
Transcriptome

ABSTRACT

Organisms suffer more harmful ultraviolet radiation in the Antarctica due to the ozone layer destruction. Bryophytes are the dominant flora in the Antarctic continent. However, the molecular mechanism of Antarctic moss adaptation to UV-B radiation remains unclear. In the research, the transcriptional profiling of the Antarctic moss *Pohlia nutans* under UV-B radiation was conducted by Illumina HiSeq2500 platform. Totally, 72,922 unigenes with N_{50} length of 1434 bp were generated. Differential expression analysis demonstrated that 581 unigenes were markedly up-regulated and 249 unigenes were significantly down-regulated. The gene clustering analysis showed that these differentially expressed genes (DEGs) includes several transcription factors, photolyases, antioxidant enzymes, and flavonoid biosynthesis-related genes. Further analyses suggested that the content of malondialdehyde (MDA), the activities of several antioxidant enzymes (i.e., catalase, peroxidase, and glutathione reductase) were significantly enhanced upon UV-B treatment. Furthermore, the content of flavonoids and the gene expression levels of their synthesis-related enzymes were also markedly increased when plants were exposed to UV-B light. Therefore, these results suggested that the pathways of antioxidant enzymes, flavonoid synthesis and photolyases were the main defense systems that contributed to the adaption of *Pohlia nutans* to the enhanced UV-B radiation in Antarctica.

1. Introduction

The terrestrial Ultraviolet-B (UV-B, wavelength 280–315 nm) is an inherent part of solar radiation and has obviously increased due to the depletion and hole of the ozone layer since about 1980 (Austin and Wilson, 2006; Mckenzie et al., 2011; Kim et al., 2015). UV-B can function as either a growth signal or an environmental stress. High UV-B irradiance will seriously restrict the growth and development of photosynthetic organisms and trigger stress-related processes, while low dose UV-B radiation mediates the plant photomorphogenesis (Lee, 2016). In Arabidopsis, the photoreceptor UV RESISTANCE LOCUS8 (UVR8) and the key signaling factor CONSTITUTIVE PHOTOMORPHOGENESIS1 (COP1) mediate the signaling pathway of UV-B perception (Tilbrook et al., 2016). Following this process, UV-B light activates the expression of the bZIP transcription factor ELONGATED HYPOCOTYL5 (HY5). Thus, the UVR8-COP1-HY5 constitute the central signaling components of signal pathway in transducing UV-B signal to adaptation response (Jenkins, 2009; Lee, 2016). COP1, functioning as an E3 ubiquitin ligase, also plays a critical role in drought stress tolerance in Arabidopsis (Moazzam-Jazi et al., 2018), suggesting there is an orchestration of stress crosstalk between UV-B and drought.

UV-B light is an important environmental factor affecting plant growth and development. Plants are autotrophic sessile organisms. Their viability was easily threatened by various abiotic stresses and most of them cannot endure the high irradiation of UV-B (Jordan, 2002; Paul and Gwynn-Jones, 2003). Since UV-B radiation damages nucleic acids (e.g., DNA) leading to the formation of pyrimidine dimmers, the transcription of cell cycle regulatory genes and DNA replication are seriously disturbed, causing genetic mutation and cell death (Jiang et al., 2011; Cadet et al., 2015; Falcone Ferreyra et al., 2016). High UV-B irradiance also produces reactive oxygen species (ROS) and reduces photosynthetic capacity leading to reductions in plant growth and productivity (Jenkins, 2009; Núñez-Pons et al., 2018). Plants have evolved and generated multiple adaptive responses to UV-B

☆ This article is part of the Special Issue "Interactive effects of UV-B radiation in a complex environment" published at the journal Plant Physiology and Biochemistry 134, 2019.

* Corresponding author. 72 Coastal Highway, Jimo District, Qingdao, 266000, Shandong, China.
E-mail address: zhangpy80@sdu.edu.cn (P. Zhang).

[1] C. Li and S. Liu are co-first authors.

https://doi.org/10.1016/j.plaphy.2018.10.034
Received 31 July 2018; Received in revised form 23 September 2018; Accepted 30 October 2018
Available online 09 November 2018

light by morphological and biochemical changes (Jiang et al., 2012). For example, UV-B radiation leads to a significant increase in total levels of secondary metabolites such as terpenoids, phenols, flavonoids, anthocyanins, alkaloids, beta-carotene, and lycopene in *Cuminum cyminum* L (Ghasemi et al., 2018). Arabidopsis transgenic plants expressing flavone synthase (i.e., *ZmFNSI* or *ZmFNSII*) accumulates apigenin, conferring protection against UV-B stress (Righini et al., 2018). In addition, UV-B acts as a stimulating factor in increasing the synthesis of several antioxidants and secondary metabolites to optimize performance under stress (Takshak and Agrawal, 2015; Matus et al., 2016). The antioxidant responses to drought in *Nicotiana benthamiana* leaves are strengthened due to the increase of flavonoids which was induced by UV-B pre-treatment (Mátai et al., 2018).

The terrestrial ecosystems in Antarctic ice free region are exposed to higher UV-B irradiation with 3.4–6.2 mW/cm^2 (Bao et al., 2018) and the plant productivity is modestly declined (estimated at < 6%) (Robinson and Erickson, 2015). Lichens and mosses are the dominant vegetation in the Antarctic continent. Reports showed that they can resist the UV-B stress using an efficient damage repair systems by synthesizing antioxidants such as UV-B-absorbing pigments and anthocyanins (Singh et al., 2010). The field experiments in Antarctica demonstrate that following prolonged UV-B exposure, total chlorophyll levels are decreased gradually in moss (*Bryum argenteum*) and lichen (*Umbilicaria aprina*), whereas the levels of UV-B absorbing compounds, phenolics, and carotenoids gradually are increased (Singh et al., 2014). In the Antarctic moss *Ceratodon purpureus*, several insoluble phenylpropanoids on cell wall function as passive UV screening compounds that enhance resistance to UV radiation (Clarke and Robinson, 2008). The biflavonoids isolated from the Antarctic moss *Ceratodon purpureus* show high antioxidant and ultraviolet-screening activity (Waterman et al., 2017). Meanwhile, the methanolic extracts containing flavonoids and carotenoids from three Antarctic species (i.e., *Polytrichum juniperinum* Hedw, *Colobanthus quitensis* (Kunth) Bartl, and *Deschampsia antarctica* Desv) display the properties of light protection which act as UV-absorbing compounds and activate the DNA-repair process (Pereira et al., 2009). Antarctic plants may use the same strategies against UV-B light as species thriving at lower latitudes. However, the molecular mechanisms that enable Antarctic plants adapting to the strong UV-B radiation are far from clearly characterized. Here, the transcriptome sequencing analyses were conducted to reveal transcriptional profiling of the Antarctic moss *Pohlia nutans* under UV-B radiation. Differentially expressed genes (DEGs) were identified and their expression levels were analyzed. Meanwhile, the content of malondialdehyde (MDA), the activities of antioxidant enzymes, and the content of total flavonoids were also measured after UV-B treatment.

2. Materials and methods

2.1. Plant samples and UV-B radiation treatments

Pohlia nutans was collected from the vicinity the Great Wall Station in Fildes Peninsula of Antarctica (S62°13.260′, W58°57.291′), in March 2014. The moss shoots with a little soil matrix were placed in vacuum-sealed plastic bags, and transport to laboratory at 4 °C. They were then cultivated in flowerpots on a soil mixture containing the Base Substrate (Klasmann-Deilmann, Germany) at 16 °C, 70% humidity, under light (70 μmol photons·m^{-2}·s^{-1}) with a 16-h-light/8-h-dark photoperiod (Liu et al., 2016). On this condition, the UV irradiance is 0.09 mW/cm^2 which is produced by Philips T8 TLD36W/54–765 fluorescent tubes.

Two Philips TL20W/01RS narrowband UV-B tubes (supplemented with Philips T8 TLD36W/54–765 fluorescent tubes) were used for UV-B treatment (Wolf et al., 2010). The average UV-B irradiance was 0.20 mW/cm^2, which determined using a UV-340A Ultraviolet Light Meter (Lutron Electronic Enterprise, Taiwan). The photosynthetically active radiation (PAR) was 1.35 μmol photons·m^{-2}·s^{-1} which measured by a LX-101A Light Meter (Lutron Electronic Enterprise, Taiwan).

Two-month-old plants were firstly adapted to a low-white light field (1.35 μmol photons·m^{-2}·s^{-1}) without UV-B irradiation for 48 h. The green gametophytes was cut off and collected as control group. Then, the other plants were treated with additional UV-B radiation (0.20 mW/cm^2) for 3 h or 6 h as the treatment group. The green gametophytes for each sample were collected and immediately frozen in liquid nitrogen, and stored at −80 °C. The plants from 3 different flowerpots were used as biological replicates. These samples were employed for the examination of transcriptome sequencing, gene expression levels, MDA content, enzyme activity assays, and flavonoid induction.

Table 1
Length distribution of assembled transcripts and unigenes.

Nucleotide length	Transcripts	Unigenes
200-500bp	57849	49175
500-1000bp	17612	9803
1000-2000bp	19833	7638
> 2000bp	17268	6306
Total	112562	72922
Min length (bp)	201	201
Mean length (bp)	983	704
Median length (bp)	477	344
Max length (bp)	12200	12200
N_{50} length (bp)	1894	1434
N_{90} length(bp)	346	260

2.2. RNA extraction and Illumina sequencing

Transcriptome sequencing were performed by Novogene Corporation (Beijing, China). Briefly, plants were treated with UV-B radiation (0.20 mW/cm^2) for 3 h and 2 g of green gametophytes were ground into power in liquid nitrogen. Total RNA was isolated by using TRIzol™ Reagent (Invitrogen, CA, USA). RNA quality were detected on 1% agarose gel electrophoresis. RNA integrity was analyzed by the Agilent 2100 Bioanalyzer (Agilent Technologies). RNA concentration was measured using Qubit® RNA Assay Kit (Life Technologies). mRNA was enriched from the total RNA by oligo (dT) magnetic beads. The purified mRNA was then broken into short fragments, which was used as template to synthesize the first- and second-strand cDNA. After reverse transcription, cDNA libraries were generated from appropriate size of DNA fragments using NEBNext® Ultra™ RNA Library Prep Kit (NEB, USA). The quality of cDNA libraries was detected by the Agilent Bioanalyzer 2100 (Agilent Technologies). Finally, the DNA fragments of cDNA libraries from three treatment groups and three control groups were clustered and sequenced on an Illumina Hiseq 2500 platform (He et al., 2018).

2.3. Transcriptome assembly, annotation and differential expression analysis

Raw reads with adaptor sequences, poly-N and low-quality reads were removed. Transcriptome assembly was implemented by Trinity software (Xu et al., 2017). Gene function was annotated using BLASTX alignment against Non-Redundant Protein Sequences (NR) and Swiss-Prot databases. Gene Ontology (GO) enrichment was performed by the GOseqR packages. KEGG pathway enrichment was implemented by using KOBAS software (Mao et al., 2005).

The gene expression levels in transcriptome sequencing were estimated by using the EdgeR package (McKenna et al., 2010). The gene expression levels were estimated with RPKM (reads per kilo base per million mapped reads). Differentially expressed genes (DEGs) analysis between UV-B treatments and control groups was implemented by using the DEGseq R package. P-value was adjusted using q value. The adjusted p-value < 0.005 and the $|\log_2(\text{Treat/Control})| > 1$ were used as the threshold to assess the significance of the differential gene expression.

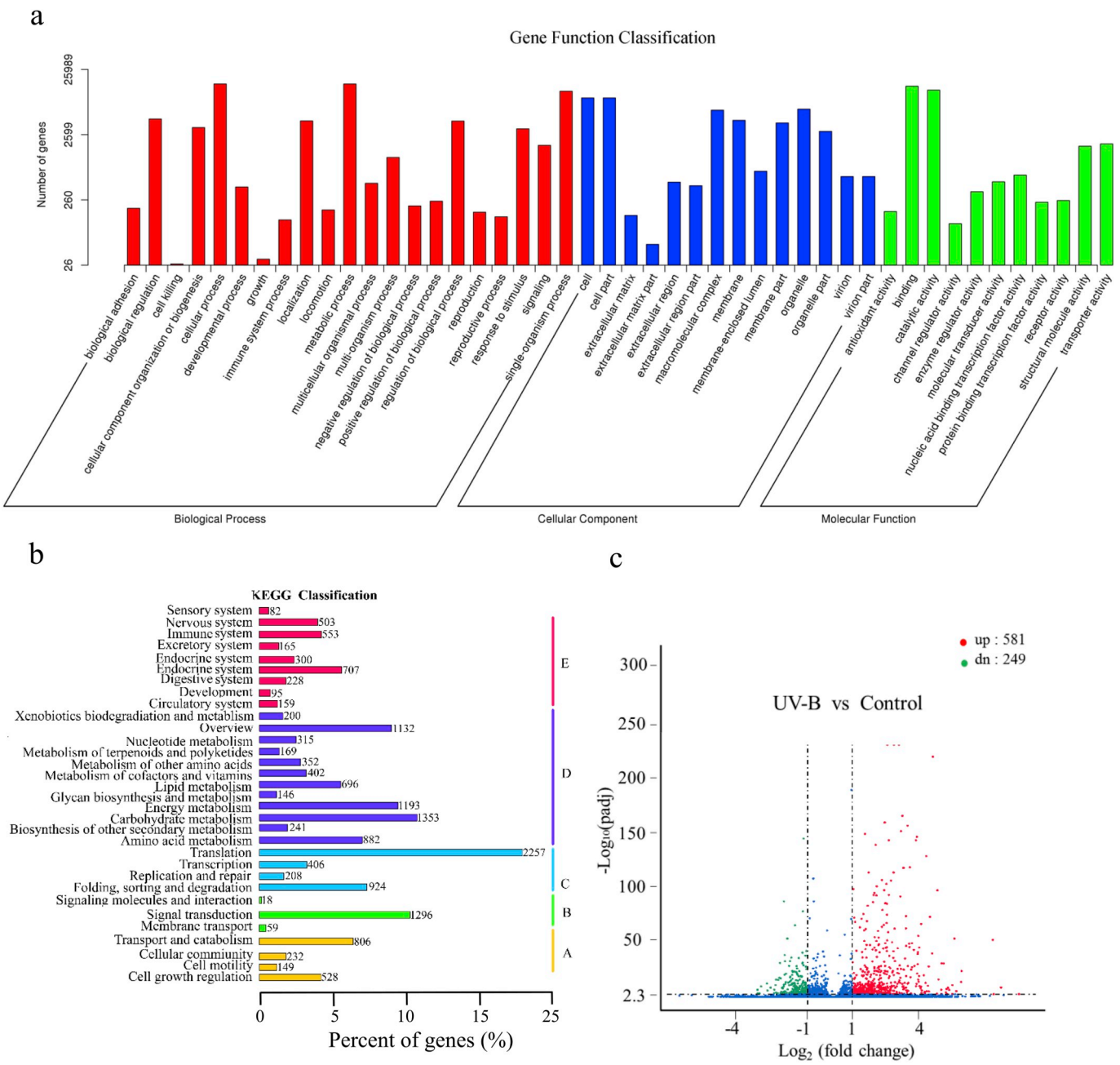

Fig. 1. Transcriptome sequencing analysis of the Antarctic moss *P. nutans* after UV-B radiation. (a) Gene Ontology classification of *P. nutans* unigenes. The vertical axis represents the number of genes in each specific category. (b) KEGG pathway enrichment of *P. nutans* Unigenes. (c) A volcano plot showing the differentially expressed genes (DEGs) between UV-B treatment groups and control groups. The X-axis means fold change of gene expression (threshold, $|\log_2(\text{Treat/Control})| > 1$). The Y-axis indicates the statistically significant level (threshold, p-value < 0.005); the smaller the adjusted pvalue (i.e., padj), the larger the $-\log_{10}(\text{padj})$, which means that the difference is more significant. Red dots indicate up-regulated genes with significant differences, and green dots indicate down-regulated genes with significant differences. Blue dots indicate genes with no significant differences. (For interpretation of the references to colour in this figure legend, the reader is referred to the Web version of this article.)

2.4. Quantitative real-time PCR analysis

To validate the reliability of the differential expression analysis, total RNA were extracted from green gametophytes after 0, 3 and 6 h of UV-B treatment. 0.5 ng of total RNA were employed for cDNAs synthesis reaction by using the PrimeScript™ RT-PCR Kit (Takara, China). The *Tubulin* gene (GenBank No. GACA01042200) from *Pohlia nutans* was identified as the most stably expressed reference genes to normalize the template. The gene specific primers were listed in Table S1. Real-time PCR analysis was run on a Stratagene Mx3000P®qPCR instrument. The cycling regime is 95 °C for 2 min, followed by 40 cycles of amplification (95 °C for 20 s, 58 °C for 20 s, and 72 °C 20 s). The reaction of each template was performed in triplicate. Relative gene expression level was calculated using the comparative Ct ($2^{-\Delta\Delta Ct}$) method (Livak and Schmittgen, 2001).

2.5. Phylogenetic analysis

HMMER program and BLASTP alignment were used to retrieve the phenylalanine ammonia lyase (PAL), chalcone synthase (CHS), chalcone isomerase (CHI), flavonoid 3′,5′-hydroxylase (F3′,5′H) 2-oxoglutarate-dependent dioxygenase (2-OGD) family genes from the

Table 2
Representative UV-B radiation-related genes of the Antarctic moss *P. nutans*.

Gene_ID	Log_2FoldChange	q-value	Gene Symbol	Functional annotation
Antioxidant enzyme				
c40186_g1	2.20	0.002930	PnCAT1	Catalase [*Gracilibacillus ureilyticu*, WP_089739773.1]
c33631_g1	1.58	1.7E-08	PnCAT2	Catalase [*Klebsormidium niten*, GAQ86405.1]
c38356_g1	4.05	0.000753	PnPOD1	Peroxidase A2-like [*Durio zibethinu*, XP_022766025.1]
c37764_g1	2.52	0.000409	PnPOD2	Peroxidase 29 [*Cicer arietinum*, XP_004507667.1]
c30931_g1	2.87	4.99E-11	PnPOD3	Peroxiredoxin-2 [*Selaginella moellendorffii*, XP_002972873.1]
c31192_g1	3.48	0.003587	PnGSH-Px1	Glutathione peroxidase [*Punica granatum*, AHN92204.1]
c54439_g1	1.52	9.02E-05	PnGSH-Px2	Glutathione peroxidase [*Volvox carteri f. nagariensis*, XP_002947348.1]
c31894_g1	2.66	2.19E-44	PnAPX1	Ascorbate peroxidase [*Grimmia pilifera*, ADF56044.1]
c34170_g1	1.88	1.54E-11	PnAPX2	L-ascorbate peroxidase 3 [*Lactuca sativa*, XP_023736344.1]
c59184_g1	2.04	0.003666	PnFeSOD1	Superoxide dismutase [Fe] [*Chlamydomonas reinhardtii,* XP_001690591.1]
c57239_g1	1.63	0.000589	PnGR1	Glutathione reductase [*Heterostelium album* PN500, XP_020432921.1]
Flavonoid synthase pathway key enzyme				
c42223_g1	3.2	1.82E-21	PnPAL1	Phenylalanine ammonia-lyase-like [*Physcomitrella patens*, XP_024394373.1]
c39509_g1	2.2	1.82E-13	PnPAL2	Phenylalanine ammonia-lyase [*Ginkgo*, ABZ04127.1]
c41330_g1	2.48	0.000035	PnCHS1	Chalcone synthase A [*Nicotiana attenuata*, XP_019231574.1]
c36006_g1	3.87	0.000536	PnCHS2	Chalcone synthase [*Arachis ipaensis*, XP_016197787.1]
c35791_g1	2.91	0.001193	PnCHI1	Chalcone isomerase 2, partial [*Conocephalum conicum*, AOC83889.1]
c41091_g1	3.06	6.29E-07	PnF3H1	Flavanone 3-dioxygenase [*Glycine soja*, KHN23297.1]
c35215_g1	4.51	2.65E-12	PnF3H2	Flavanone 3-hydroxy [*Arabidopsis thaliana*, AT3G51240.1]
c35939_g1	1.8	0.000286	PnFLS1	Flavonol synthase/flavanone 3-hydroxylase-like [*Prunus avium*, XP_021810338.1]
c37498_g1	3.27	0.003651	PnFLS2	Flavonol synthase/flavanone 3-hydroxylase [*Arabidopsis thaliana*, AT5G08640.2]
c39650_g1	2.02	1.07E-10	PnF3′,5′H1	Flavonoid 3′,5′-hydroxylase [*Delphinium chefoense*, AQL59239.1]
c33956_g1	2.86	3.43E-08	PnLDOX1	Leucoanthocyanidin dioxygenase [*Ananas comosu*, OAY80609.1]
UV-B signaling pathway and DNA repair system gene				
c34874_g1	1.93	1.12E-06	PnUVR8-1	UVB-resistance protein UVR8 [*Arabidopsis thaliana*, AAD43920.1]
c42638_g1	2.53	6.61E-12	PnUVR8-2	Ultraviolet-B receptor UVR8-like [*Physcomitrella patens*, XP_024371209.1]
c39904_g1	2.21	1.58E-46	PnUVR3	UVR3 [*Arabidopsis thaliana*, OAP02498.1]
c40253_g1	3.7	7.04E-31	PnHY5	Transcription factor HY5 [*Manihot esculenta*, XP_021597568.1]
c37574_g1	3.95	0.003815	PnCOP1-1	E3 ubiquitin-protein ligase COP1 [*Nelumbo nucifera*, XP_010252572.1]
c38764_g1	3.33	1.37E-10	PnCOP1-2	COP1 [*Ipomoea batatas*, AOQ25826.1]
c41725_g1	2.14	1.43E-29	PnRUP2	WD repeat-containing protein RUP2 [*Jatropha curcas*, XP_012090270.1]
c16819_g1	2.84	0.00147	PnMSH1	DNA mismatch repair protein MSH1, mitochondrial-like [*Physcomitrella patens*, XP_024383551.1]
c39994_g1	4.85	0.001777	PnPHR-1	AtPHR1-like type 2 CPD DNA photolyase [*Physcomitrella patens,* XP_001764990.1]
c43268_g1	1.98	0.000027	PnPHR-2	Blue-light photoreceptor PHR2 [*Arachis ipaensis*, XP_016184459.1]
Other stress-related gene				
c40577_g1	−1.12	1.12E-35	PnMYB	R2R3MYB9 [*Ginkgo biloba*, ASR18094.1]
c33446_g1	4.46	0.000788	PnDREB-1	Dehydration-responsive element-binding protein 5-2 [*Syntrichia caninervis*, AMT92110.1]
c34009_g1	1.26	2.99E-10	PnDREB-2	Dehydration-responsive element-binding protein 5-9 [*Syntrichia caninervis*, AMT92117.1]
c41834_g1	1.39	2.52E-34	PnERF	Ethylene-responsive transcription factor RAP2-4-like [*Ipomoea nil*, XP_019177314.1]
c40620_g1	1.32	8.16E-48	PnABI5	ACID-INSENSITIVE 5-like protein 5 [*Morus notabilis*, XP_010112189.1]
c39444_g1	3.92	6.47E-15	PnNCED	Putative 9-cis-epoxycarotenoid dioxygenase [*Cryptomeria japonica*, BAF31905.1]
c40908_g1	−1.35	0.000732	PnLOX5	Lipoxygenase-5 [*Physcomitrella patens*, ABF66651.1]
c39519_g1	1.81	0.000166	PnOPR11	Putative 12-oxophytodienoate reductase 11 [*Manihot esculenta*, XP_021601480.1]
c36631_g1	1.88	0.000017	PnGA20ox	Gibberellin 20-oxidase [*Physcomitrella patens*, XP_001759112.1]

Antarctic moss transcriptome. Their homologous protein sequences of other land plants were obtained from GenBank. The G protein-coupled receptor protein (GPCR, AAB49751.1) was used as outgroup in the tree. Multiple alignments of these family proteins were performed using the ClustalW program. The phylogenetic analysis was performed by the neighbor-joining method using the Mega 5.0 software (Tamura et al., 2011). The bootstrap values of each branch in phylogeny tree was generated by1000 bootstrap replicate.

2.6. The MDA content, enzyme CAT, GR, POD activities, and flavonoid content

Mosses were irradiated by UV-B tubes and the average UV-B irradiance was 0.20 mW/cm^2 as described above. After UV-B treatment, 0.5 g of the moss gametophytes were cut off and frozen immediately in liquid nitrogen. Then, plant samples were ground in an ice-cold mortar with 5 mL potassium phosphate buffer (50 mM, pH 7.4). The mixture was centrifuged at 12000 g for 10 min at 4 °C. The supernatant was used for detecting the Malondialdehyde (MDA) contents and the enzyme activity assays of Catalase (CAT), Peroxidase (POD) and Glutathione reductase (GR) using the commercial assay kits (Nanjing Jiancheng Bioengineering Institute, Nanjing, China). The experiments were repeated three times.

The total flavonoids were isolated from green gametophytes by using the extraction kit. In brief, the Antarctic moss samples (20 mg dry wt) were extracted with ethanol solution (60%, 1 mL) under 60 °C, ultrasonic oscillation for 3 h. After centrifugation at 12,000 rpm for 20 min, the upper aqueous phase with flavonoids was transferred to a clean tube. Then, the extractions were mixed with the reagent solution, and kept at room temperature for 30 min. Finally, the absorbance was detected at the wavelength of 405 nm using a UV–visible spectrophotometer (Shimadzu, Japan, UV-2450). The experiments were repeated three times.

2.7. Statistical analysis

The experiments were conducted in three biological replicates and all data presented as the mean (± SD). Significant statistical difference between the UV-B treatment and the control group was analyzed using Student's *t*-test (*$P < 0.05$, **$P < 0.01$).

3. Result

3.1. Transcriptome sequencing and assembly

The transcriptome of *P. nutans* was sequenced on an Illumina Hiseq

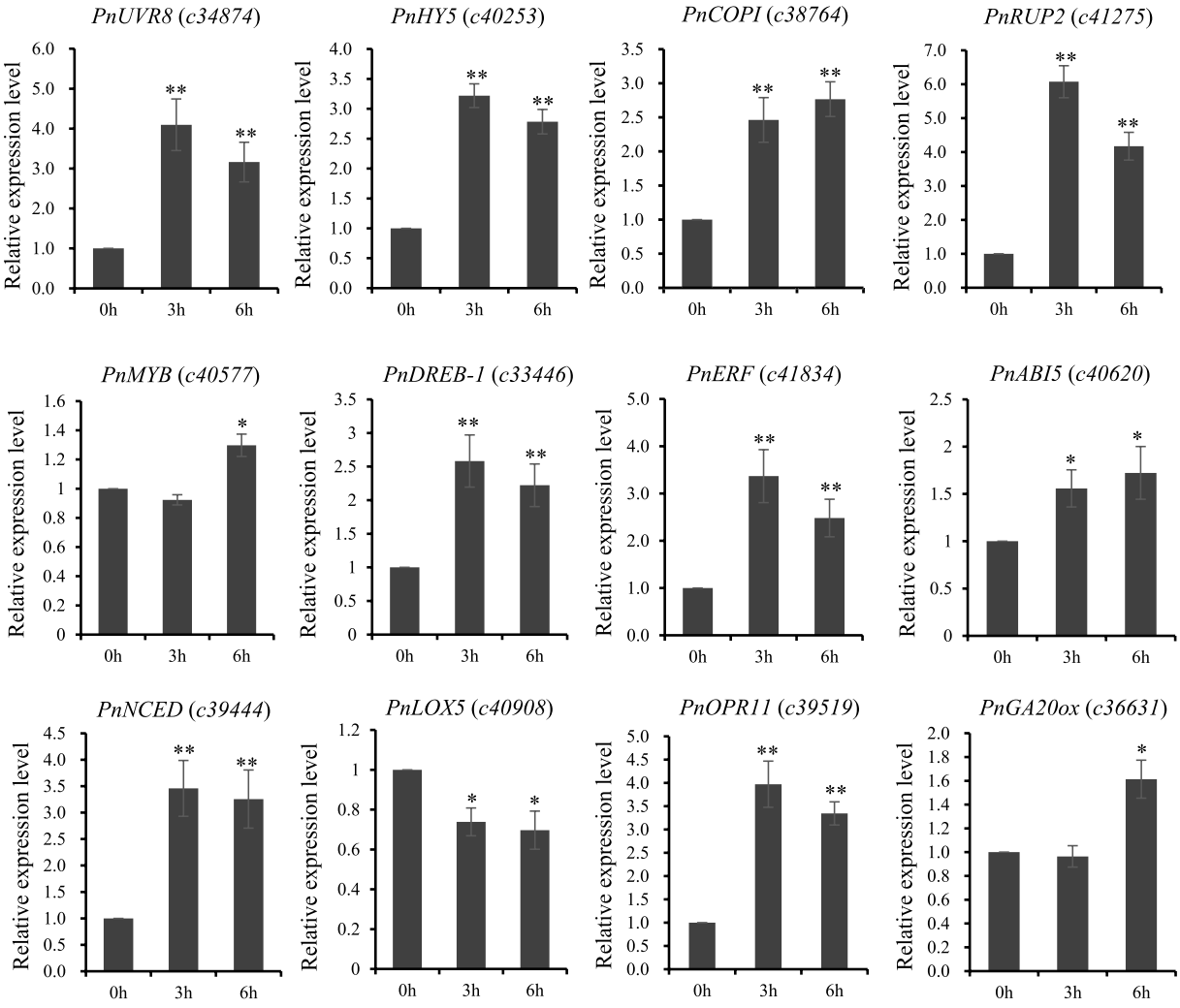

Fig. 2. Verification and analysis of the gene expression levels via quantitative real-time PCR. The Y-axis refer to the relative expression level. The X-axis represent 0, 3, and 6 h UV-B radiation. Vertical bars indicate the means ± SD of three replicates of the sample. Asterisks indicate significant differences between the means of the UV-B radiation groups and the control groups (*$P < 0.05$, **$P < 0.01$).

2500 platform. A total of 112,562 transcripts ranging from 200 bp to 12,200 bp were assembled; the average length was 983 bp, the N_{50} and the N_{90} were 1894 bp and 346 bp, respectively. A total of 72,922 unigenes (non-redundant sequences) were generated and the length distribution of unigenes was analyzed. Among the unigenes, 67.43% was between 100 and 500 bp, 13.44% was 0.5–1 kb, 10.47% was 1–2 kb, and the remaining 8.64% was longer than 2 kb (Table 1).

3.2. Functional annotation and classification

Gene function was annotated by BLAST against the databases of Nr, KOG, and SWISS-PROT. Then, a total of 25,989 unigenes were classified into the categories of biological process (BP), cellular component (CC), and molecular function (MF) and further distributed into 46 functional subgroups (Table 1). In biological process, cellular process (15,572 unigenes) was the most highly represented GO terms, followed by metabolic process (15,556 unigenes) and single-organism process (12,045 unigenes). In cellular component, the majority of unigenes were involved in cell (9517 unigenes) and cell part (9516 unigenes). In molecular function, these unigenes were predominantly distributed binding (1,4374 unigenes) and catalytic activity (12,522 unigenes) (Fig. 1a). The metabolic pathway analysis showed that a total of 12,998 unigenes were divided into cellular processes, environmental information processing, genetic information processing, metabolism, etc. (Fig. 1b). Translation group (2257 unigenes) was mostly enriched, followed by these for Carbohydrate metabolism (1353 unigenes) and signal transduction (1296 unigenes).

3.3. Differential expression analysis

A total of 830 DEGs were identified by differential expression analysis (Fig. 1c). The differentially expressed genes were classified according to their function, which involved in ROS scavenging, flavonoid synthesis, UV-B signaling, and DNA repair. The representative differentially expressed genes were shown in Table 2.

The reliability of differential expression analysis was validated using the specific primers (Supplementary Table S1) and real-time PCR technique. The results showed that transcription factor (*PnDREB*, and *PnERF*), UV-B signaling pathway genes (*PnUVR8*, *PnHY5*, *PnCOP1*, and *PnRUP2*), and DNA repair system genes (*PnPHR*) were significantly up-regulated after 3 h of UV-B treatment, which were consistent with transcriptome data. In addition, the phytohormone related genes such as *PnNCED*, *PnLOX5*, *PnABI5*, and *PnOPR11* were also up-regulated after 3 h or 6 h of UV-B treatment. But the expression levels of *PnGA20ox* were not in accordance with the differential expression analysis (Fig. 2). Therefore, real-time PCR analysis showed that the results of differential expression analysis were generally accurate and reliable.

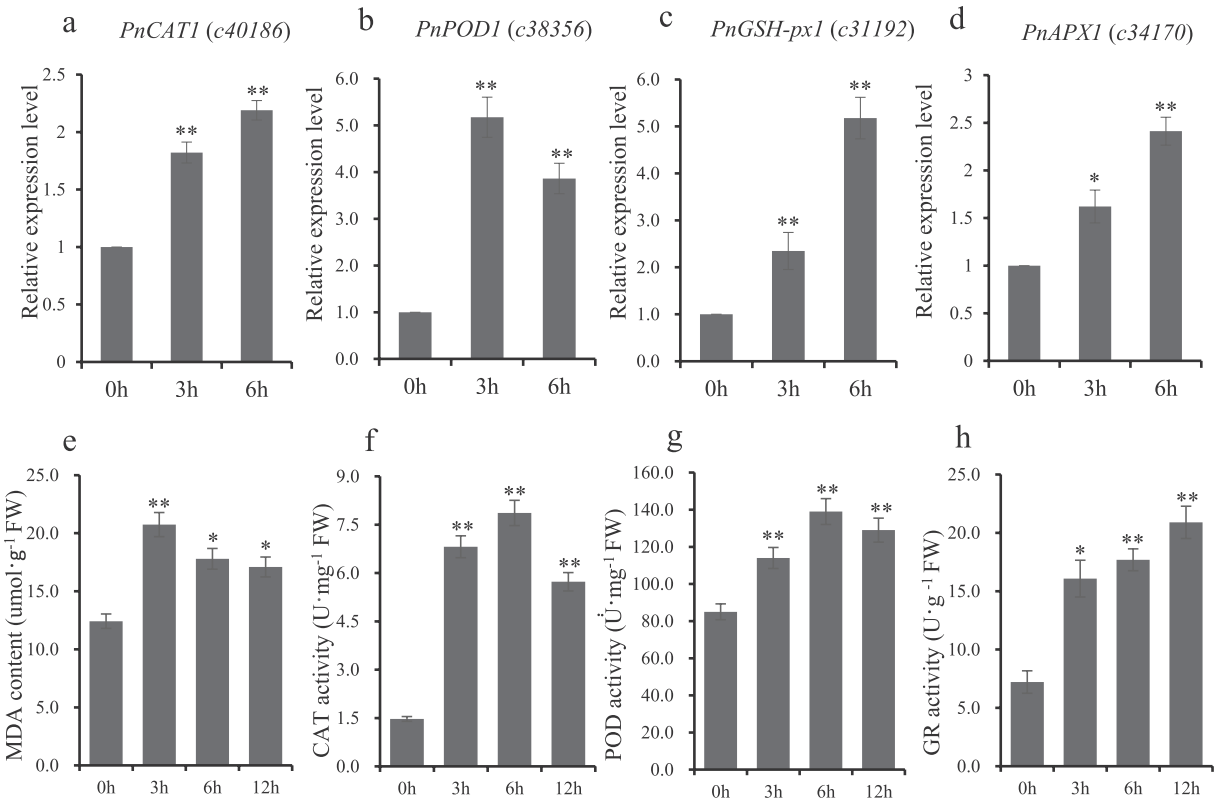

Fig. 3. Antioxidation analysis of the Antarctic moss *P. nutans* after UV-B radiation. (a) *PnCAT1*, (b) *PnPOD1*, (c) *PnGSH-px1*, and (d) *PnAPX1* expression were analyzed by quantitative real-time PCR. (e) MDA content; (f) CAT activity; (g) POD activity; (h) GR activity. The X-axis indicates UV-B treatment time; the Y-axis indicates the physiological activities. Vertical bars are means ± SD, and asterisks indicate significant differences between the means of the UV-B radiation groups and the control groups (*$P < 0.05$, **$P < 0.01$).

3.4. Antioxidant capacity assay of P. nutans under UV-B radiation

UV-B radiation leads to DNA damage that produces oxygen free radicals, and further leads to oxidative stress (Tuteja et al., 2001; Rold-Anarjona and Ariza, 2009). Antioxidant enzymes are the main oxygen free radical scavengers. In differential expression analysis, two CAT, three POD, Two GSH-Px, Two APX, one FeSOD, and one GR were significantly up-regulated (Table 2). Real-time PCR analysis showed that the gene expression levels of *PnCAT1, PnPOD1, PnGST-PX1,* and *PnAPX1* were up-regulated in *P. nutans* after UV-B radiation (Fig. 3a–d). Furthermore, physiological analysis showed that the enzyme activities of CAT, POD, and GR were significantly increased after UV-B radiation (Fig. 3f–h). Meanwhile, the content of MDA was increased to 20.73 μmol g^{-1} after UV-B radiation for 3 h, which was significantly higher than that of the control group (12.42 μmol g^{-1}) (Fig. 3e).

3.5. Phylogenetic analysis of key enzymes in flavonoid biosynthesis

The key enzymes involved in flavonoid synthesis were identified from the Antarctic moss *P. nutans* transcriptome, including two PAL, four CHS, three CHI, four F3′,5′H, and seven 2-OGD genes. The phylogenetic analysis of these enzymes showed that the PAL, CHS, CHI, F3′, 5′H, and 2-OGD family genes clustered in each clade. In CHS phylogenetic clade, the PnCHS4 kept relatively closer with the PpCHS, while other PnCHS genes (i.e., c39025, c41330 and c36006) clustered together with the AtCHS (AED91961.1). Flavonol synthase, flavanone-3-hydroxylase, and anthocyanidin synthase all have the 2OG-FeII_Oxy domain and DIOX_N domain, belonging to the 2-oxoglutarate-dependent dioxygenase (2-OGD) superfamily. We isolated seven 2-OGD genes from *P. nutans* transcriptome including three FLS, two F3H, and two ANS. The phylogenetic analysis showed that they were mainly divided into three subgroups (Fig. 4). However, the functions of these enzymes need to be further analyzed by employing in *vitro* enzyme activity assay.

3.6. Flavonoid biosynthesis assay of P. nutans under UV-B radiation

Flavonoid biosynthesis requires a series of enzymes to catalyze. The differential expression analysis showed that several enzymes of the phenylpropanoid and flavonoid biosynthesis pathway, including PAL, CHI, CHS, 2-OGD, and F3′,5′H were up-regulated after UV-B radiation (Table 2). Real-time PCR analysis confirmed that the flavonoid-related genes (*PnPAL1*, *PnPAL2*, *PnCHS1*, *PnCHS2*, *PnCHI1*, *PnCHI2*, *PnF3H1*, *PnF3H2*, *PnFLS1*, *PnFLS2*, *PnF3′,5′H1*, and *PnANS1*) were up-regulated after UV-B radiation, which were consistent with the transcriptome sequencing data. Furthermore, the content of total flavonoids in *Pohlia nutans* was measured. The result showed that the flavonoid content was 2.87 mg g^{-1} at 96 h of UV-B radiation, which is 1.65-fold that of the control group (Fig. 5).

4. Discussion

Moss, as the main terrestrial flora in the Antarctic continent, may be helpful material for studying the response mechanisms of plants to UV-B radiation (Clarke and Robinson, 2008). Here, the transcriptome of the Antarctic moss *P. nutans* was sequenced and analyzed on an Illumina Hiseq 2500 platform. 112,562 transcripts and 72,922 unigenes were generated after transcriptome assembly, their N_{50} lengths were 1894 bp and 1434 bp, respectively (Table 1). Antarctic plants seem to possess similar mechanism of UV-B signaling, photoprotection and damage repair as those found in vascular plants (e.g., Arabidopsis and rice) (Núñez-Pons et al., 2018). The differential expression analysis showed that 581 genes were up-regulated and 249 genes were down-regulated after UV-B

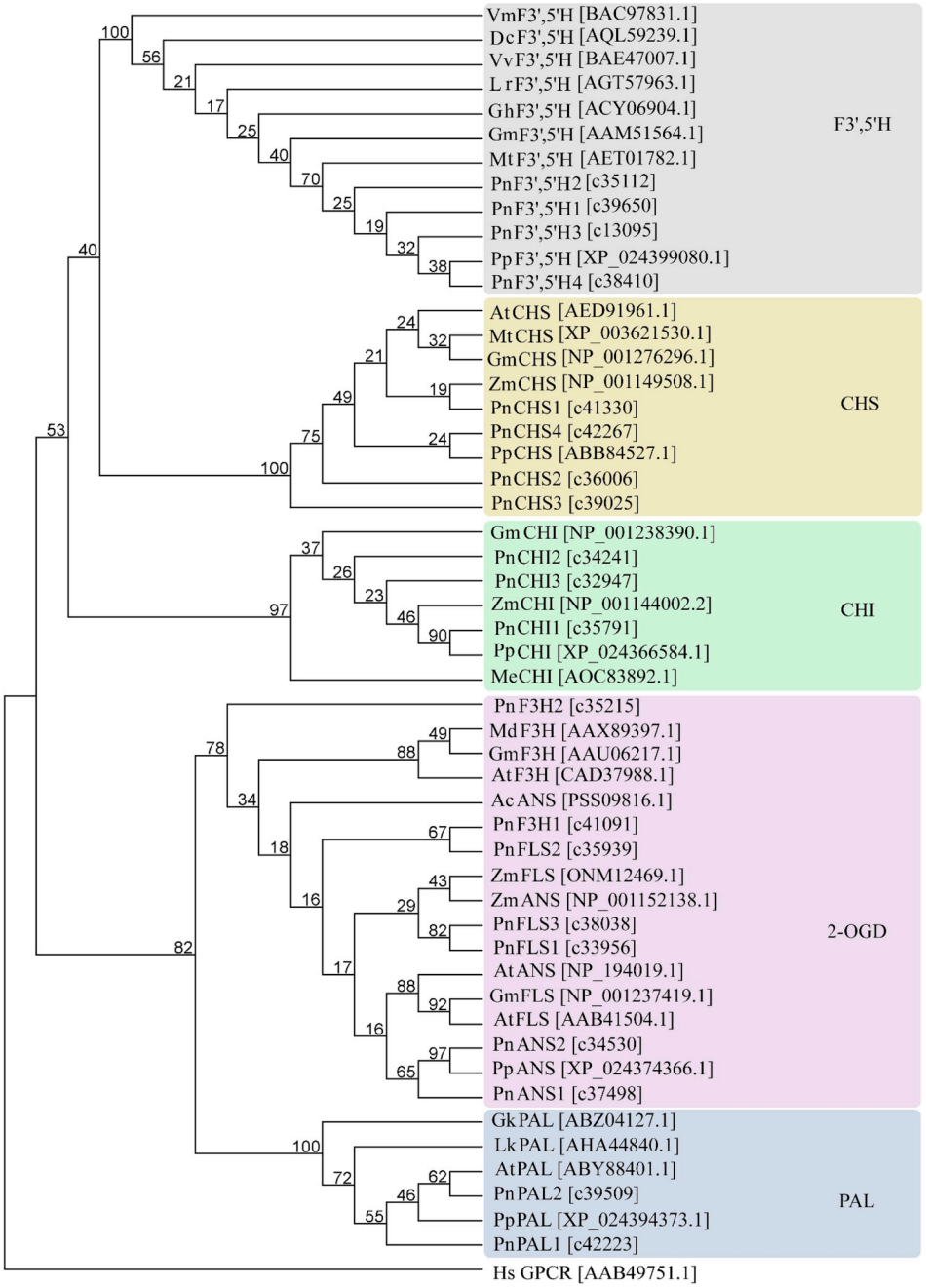

Fig. 4. Phylogenetic analysis of PAL, CHI, CHS, F3′,5′H, and 2-OGD family proteins.

treatment (Fig. 1c). These DEGs comprised of multiple pathways of UV-B stress-related genes, including ROS scavenging, flavonoid synthesis, UV-B signaling, and DNA repair (Table 2). Several transcriptional factors (TFs) were demonstrated to mediate the signaling pathway in response to abiotic stress, including MYBs, NACs, AP2/ERF, bHLHs, and bZIPs (Fujita et al., 2011; Shi et al., 2014; Li et al., 2016). The bZIP transcription factor HY5, a key moderator of photomorphogenesis, acts downstream of the UV-B photoreceptor UVR8 in response to UV-B radiation (Jenkins, 2009; Binkert et al., 2014; Lee, 2016). UVR8 is a positive regulator of UV-B-induced photomorphogenic responses (Favory et al., 2009; Liu et al., 2016). When plants perceived UV-B radiation, UVR8 transformed from homodimeric form into monomer and interacted with E3 ubiquitin ligase. In this study, DEGs and real-time PCR analysis showed that *PnHY5* and *PnUVR8* in *Pohlia nutans,* which involved in the UV-B signal perception and transduction pathway, were up-regulated after UV-B stress (Table 2 and Fig. 2).

High fluence UV-B severely damaged the DNA, proteins, and membranes lipids (Heck et al., 2003; Ulm and Nagy, 2005). Correspondingly, plants have formed multiple mechanisms to cope with these deleterious effects, such as DNA-repair system, antioxidant system and UV-absorbing phenolic compounds (Lee, 2016). In the present study, the DNA repair system genes (i.e., CPD photolyase *PnPHR1*, *PnPHR2*) and DNA mismatch repair gene (i.e., *PnMSH1*) were up-regulated, which implied that these gene involved in reducing the DNA damage that caused by UV-B radiation (Table 2). The content of MDA was significantly increased after UV-B radiation, suggesting that oxidative damage was one of the deleterious effects (Fig. 3e). Meanwhile, the activities of several antioxidant enzymes such as CAT, POD, and APX were significantly increased in the Antarctic moss *P. nutans* after UV-B radiation, conferring for removing the free radicals (Fig. 3f–h).

Flavonoids play important biological functions during plant development and abiotic stress. PAL is the rate-limiting enzyme which

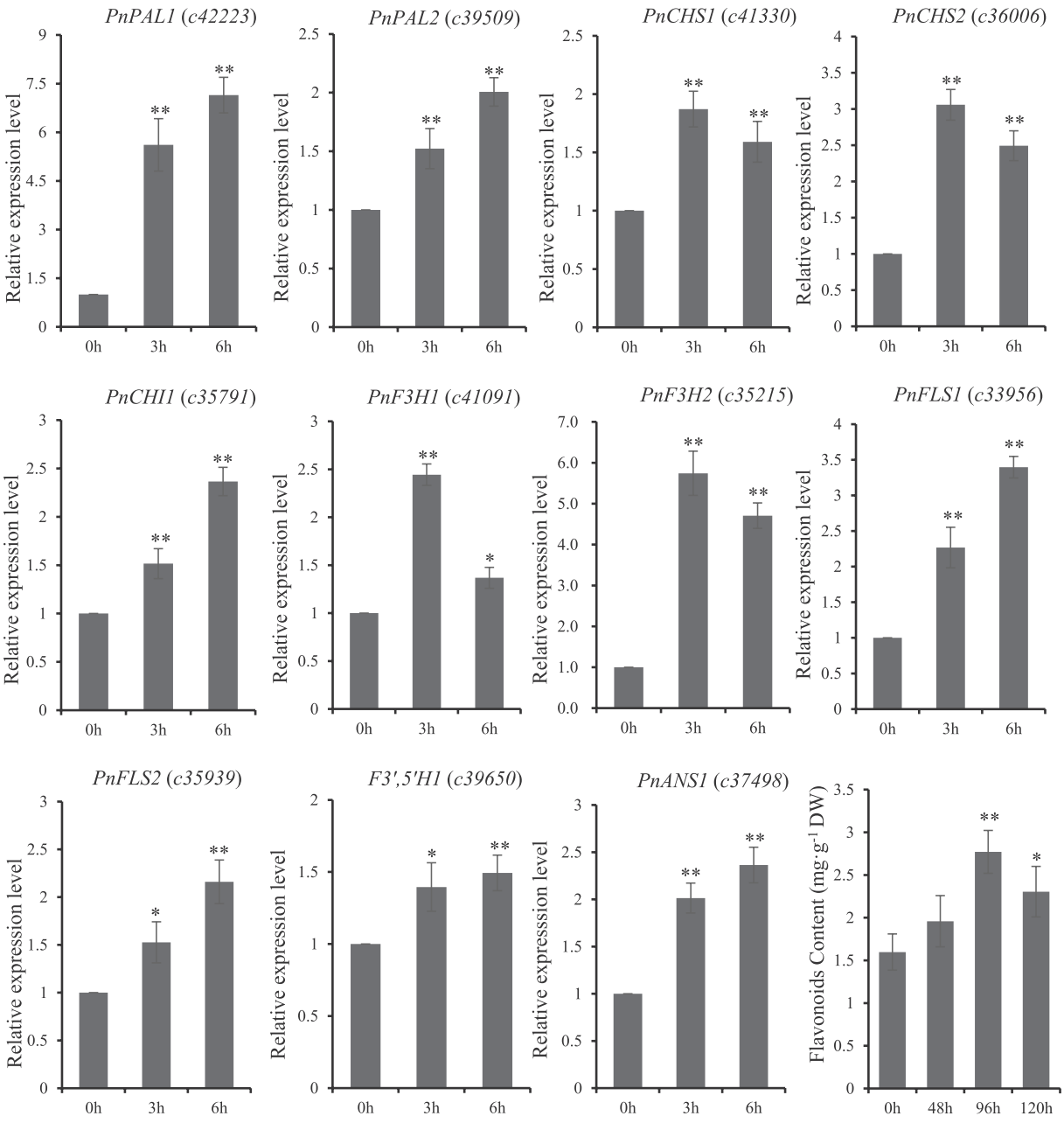

Fig. 5. Flavonoid biosynthesis pathway was up-regulated by UV-B radiation. The expression levels of flavonoid-related genes (i.e., *PAL*, *CHS*, *FLS*, *ANS* and *F3′,5′H*) were analyzed by real-time PCR. The content of flavonoid was measured. The X-axis indicates UV-B treatment time; the Y-axis indicates the relative expression level. The data were obtained from three independent experiments. Vertical bars are means ± SD, and Asterisks indicate significant differences between the means of the UV-B radiation groups and the control groups (*$P < 0.05$, **$P < 0.01$).

catalyzes phenylalanine deamination to trans-cinnamic acid and controls the entire flux of the phenylpropanoid metabolism (Yang et al., 2015; Li et al., 2017b). CHS catalyzes the first step reaction of flavonoids and is induced by distinct UV-B and UV-A/blue light signal in Arabidopsis (Christie and Jenkins, 1996). The expression of *PAL* and *CHS* were induced by UV-B radiation in *Physcomitrella patens* (Wolf et al., 2010). However, the downstream metabolism pathways of flavanone (such as naringenin) in bryophytes are largely not documented (Li et al., 2017a). One major cause is that the flavanone metabolism enzymes (i.e., F3H, FNSI, FLS, and ANS) have same conserved protein domain, belonging to 2-oxoglutarate-dependent dioxygenase (2-OGD) family protein (Kawai et al., 2014). Their functions need to be identified by in vitro enzyme activity assay and in vivo gene overexpression or knockout approach. In the present study, seven candidates of 2-OGD genes were identified in *P. nutans* transcriptome that might participate in flavonoid biosynthesis (Table 2 and Fig. 5).

The biosynthesis of UV-B absorbing pigments and flavonoid compounds is deemed to serve as non-enzymatic antioxidants and protect plants from UV-B radiation in Antarctica (Singh et al., 2010). More than 219 novel natural products were described since 2001, from the polar microoganisms, moss, lichen, and marine faunas (Tian et al., 2017). In the present study, the transcriptome sequencing analysis also showed that several key enzymes in secondary metabolites were involved in UV-B radiation (Table 2). Real-time PCR analysis showed that *PAL*, *CHS*, *CHI*, *2-OGD* (i.e., *FLS*, *F3H*, and *ANS*), *F3′,5′H* were up-regulated after UV-B radiation (Fig. 5). Moreover, the total flavonoid contents were also increased in the *P. nutans* after UV-B radiation. In moss model plant *P. patens*, the flavonoid biosynthesis-related genes (i.e., five PAL, one 4CL, one CHI, and two CHS) are upregulated after 1 h of UV-B radiation. In addition, the content flavonols are increased in *P. patens*,

probably functioning as UV-B "sunscreens" (Wolf et al., 2010). UV-B irradiation also increases the production of anthocyanins in Arabidopsis, with broad-band UV-B being more effective. However, in *P. patens*, anthocyanins can't be detected in methanolic extracts separated by high-performance thin-layer chromatography (Wolf et al., 2010). Furthermore, F3H and FNS homologous genes are not found in *P. patens* genome (Kawai et al., 2014). However, FNS I, isolated from the liverwort *Plagiochasma appendiculatum*, shows flavanone 2-hydroxylase activity catalyzing the conversion of naringenin to apigenin and 2-hydroxynaringenin (Han et al., 2014). Our previously study showed that PnF3H, a flavanone 3-hydroxylase from *P. nutans*, induces the catabolism of naringenin and enhances plant tolerance to salt stress (Li et al., 2017a). Therefore, although the existence of UV-B-dependent induction of flavonoid biosynthesis in bryophytes contributes to the water-to-land transition of plants (Wolf et al., 2010), it is still uncertain whether bryophytes can synthesize the downstream molecules of flavonoids (e.g., anthocyanins).

Antarctic mosses and lichens have been found to develop diverse stress resistance genes and novel secondary metabolites during evolutionary process against the extreme environment (Tian et al., 2017). In this study, approximately 30 stress-related genes were identified from the Antarctic moss *P. nutans* transcriptome. We proposed that DNA-repair system, antioxidant system, and flavonoid biosynthesis pathway collectively contribute to the Antarctic moss *P. nutans* adapting to UV-B radiation, protecting cell from DNA damage and remove free radicals. Future studies will focus on the phylogenetic evolution of the flavonoid pathway in the Antarctic mosses, medical efficacy assay of flavonoids, and validating for stress resistance genes in improving plant resistance by transgenic approaches.

Conflicts of interest

The authors declare that there is no competing interests in the submission.

Author contributions

Chengcheng Li performed most of the experiments. Shenghao Liu sampled the materials, analyzed the data, and wrote the original draft. Wei Zhang participated in the phylogenetic analysis using MEGA software. Kaoshan Chen participated in experimental design and supervision. Pengying Zhang conceived and designed the experiments, reviewed & edited the manuscript, acquired funding, and administrate projects. All authors read and approved the final version of the article.

CRediT authorship contribution statement

Chengcheng Li: Formal analysis. **Shenghao Liu:** Writing – original draft. **Wei Zhang:** Data curation. **Kaoshan Chen:** Supervision. **Pengying Zhang:** Funding acquisition.

Acknowledgments

This work was supported by the National Natural Science Foundation of China (41476174 and 41206176), the Natural Science Foundation of Shandong Province of China (ZR2017MD013), the Excellent Creative Team Fund of Jinan of China, and the Fund project for transformation of agricultural scientific and technological achievements of Shandong Province of China.

Appendix A. Supplementary data

Supplementary data to this article can be found online at https://doi.org/10.1016/j.plaphy.2018.10.034.

The phylogenetic trees was constructed by the neighbor-joining method using MEGA 5.0.1000 bootstrap replicates were used in phylogeny tree analysis. Gm, *Glycine max*; Lr, *Lycium ruthenicum*; Vv, *Vitis vinifera*; Dc, *Delphinium chefoense*; Gh, *Gossypium hirsutum*; Vm, *Vinca major*; Pn, *Pohlia. nutans*; Pp, *Physcomitrella patens*; Mt, *Medicago truncatula*; At, Arabidopsis *thaliana*; Zm, *Zea mays*; Me, *Marchantia emarginata*; Lk, *Larix kaempferi*; Gk, *Ginkgo*; Md, *Malus domestica*; Ac, *Actinidia chinensis var. chinensis*; Hs, *Homo sapiens*.

References

Austin, J., Wilson, R.J., 2006. Ensemble simulations of the decline and recovery of stratospheric ozone. J. Geophys. Res. 111, 1–16.
Bao, T., Zhu, R., Wang, P., Ye, W., Ma, D., Xu, H., 2018. Potential effects of ultraviolet radiation reduction on tundra nitrous oxide and methane fluxes in maritime Antarctica. Sci. Rep. 8, 3716.
Binkert, M., Kozma-Bognár, L., Terecskei, K., De Veylder, L., Nagy, F., Ulm, R., 2014. UV-B-responsive association of the Arabidopsis bZIP transcription factor ELONGATED HYPOCOTYL5 with target genes, including its own promoter. Plant Cell 26, 4200–4213.
Cadet, J., Grand, A., Douki, T., 2015. Solar UV radiation-induced DNA Bipyrimidine photoproducts: formation and mechanistic insights. Top. Curr. Chem. 356, 249–275.
Christie, J.M., Jenkins, G.I., 1996. Distinct UV-B and UV-A/Blue light signal transduction pathways induce chalcone synthase gene expression in Arabidopsis Cells. Plant Cell 8, 1555–1567.
Clarke, L.J., Robinson, S.A., 2008. Cell wall-bound ultraviolet-screening compounds explain the high ultraviolet tolerance of the Antarctic moss, *Ceratodon purpureus*. New Phytol. 179, 776–783.
Falcone Ferreyra, M.L., Casadevall, R., D'Andrea, L., AbdElgawad, H., Beemster, G.T., Casati, P., 2016. AtPDCD5 plays a role in programmed cell death after UV-B exposure in Arabidopsis. Plant Physiol. 170, 2444–2460.
Favory, J.J., Stec, A., Gruber, H., Rizzini, L., Oravecz, A., Funk, M., Albert, A., Cloix, C., Jenkins, G.I., Oakeley, E.J., 2009. Interaction of COP1 and UVR8 regulates UV-B-induced photomorphogenesis and stress acclimation in Arabidopsis. EMBO J. 28, 591–601.
Fujita, Y., Fujita, M., Shinozaki, K., Yamaguchishinozaki, K., 2011. ABA-mediated transcriptional regulation in response to osmotic stress in plants. J. Plant Res. 124, 509–525.
Ghasemi, S., Kumleh, H.H., Kordrostami, M., 2018. Changes in the expression of some genes involved in the biosynthesis of secondary metabolites in *Cuminum cyminum* L. under UV stress. Protoplasma. https://doi.org/10.1007/s00709-018-1297-y.
Han, X.J., Wu, Y.F., Gao, S., Yu, H.N., Xu, R.X., Lou, H.X., Cheng, A.X., 2014. Functional characterization of a *Plagiochasma appendiculatum* flavone synthase I showing flavanone 2-hydroxylase activity. FEBS Lett. 588, 2307–2314 2014.
He, B., Ma, L., Hu, Z., Li, H., Ai, M., Long, C., Zeng, B., 2018. Deep sequencing analysis of transcriptomes in *Aspergillus oryzae* in response to salinity stress. Appl. Microbiol. Biotechnol. 102, 897–906.
Heck, D.E., Vetrano, A.M., Mariano, T.M., Laskin, J.D., 2003. UVB light stimulates production of reactive oxygen species: unexpected role for catalase. J. Biol. Chem. 278, 22432–22436.
Jenkins, G.I., 2009. Signal transduction in responses to UV-B radiation. Annu. Rev. Plant Biol. 60, 407.
Jiang, L., Wang, Y., Björn, L.O., Li, S., 2011. UV-B-induced DNA damage mediates expression changes of cell cycle regulatory genes in Arabidopsis root tips. Planta 233, 831–841.
Jiang, L., Wang, Y., Björn, L.O., He, J.X., Li, S., 2012. Sensing of UV-B radiation by plants. Plant Signal. Behav. 7, 999–1003.
Jordan, B.R., 2002. Review: molecular response of plant cells to UV-B stress. Funct. Plant Biol. 29, 909–916.
Kawai, Y., Ono, E., Mizutani, M., 2014. Evolution and diversity of the 2-oxoglutarate-dependent dioxygenase superfamily in plants. Plant J. 78, 328–343.
Kim, K.D., Min, Y.Y., Jin, H.S., Yang, J.K., Kim, M.Y., Lee, S.H., 2015. Underlying genetic variation in the response of cultivated and wild soybean to enhanced ultraviolet-B radiation. Euphytica 202, 207–217.
Lee, J.H., 2016. UV-B signal transduction pathway in Arabidopsis. J. Plant Biol. 59, 223–230.
Li, C.C., Liu, S.H., Yao, X.H., Wang, J., Wang, T., Zhang, Z.H., Zhang, P.Y., Chen, K.S., 2017a. PnF3H, a flavanone 3-hydroxylase from the Antarctic moss *Pohlia nutans*, confers tolerance to salt stress and ABA treatment in transgenic Arabidopsis. Plant Growth Regul. 83, 489–500.
Li, J., Lv, X., Wang, L., Qiu, Z., Song, X., Lin, J., Chen, W., 2017b. Transcriptome analysis reveals the accumulation mechanism of anthocyanins in 'Zijuan' tea (*Camellia sinensis* var. asssamica (Masters) kitamura) leaves. Plant Growth Regul. 81, 1–11.
Li, J., Yang, P., Kang, J., Gan, Y., Yu, J., Calderón-Urrea, A., Jian, L., Zhang, G., Feng, Z., Xie, J., 2016. Transcriptome analysis of pepper (*Capsicum annuum*) revealed a role of 24-Epibrassinolide in response to chilling. Front. Plant Sci. 7, 1281.
Liu, S., Wang, J., Chen, K., Zhang, Z., Zhang, P., 2016. The L-type lectin receptor-like kinase (*PnLecRLK1*) from the Antarctic moss *Pohlia nutans* enhances chilling-stress tolerance and abscisic acid sensitivity in Arabidopsis. Plant Growth Regul. 81, 409–418.
Livak, K.J., Schmittgen, T.,D., 2001. Analysis of relative gene expression data using real-time quantitative PCR and the $2^{-\Delta\Delta Ct}$ Method. Methods 25, 402–408.
Mao, X., Cai, T., Olyarchuk, J.G., Wei, L., 2005. Automated genome annotation and pathway identification using the KEGG Orthology (KO) as a controlled vocabulary. Bioinformatics 21, 3787–3793.

Mátai, A., Nagy, D., Hideg, É., 2018. UV-B strengthens antioxidant responses to drought in *Nicotiana benthamiana* leaves not only as supplementary irradiation but also as pre-treatment. Plant Physiol. Biochem. S0981–9428 30413-30413.

Matus, J.T., 2016. Transcriptomic and metabolomic networks in the grape berry illustrate that it takes more than flavonoids to fight against ultraviolet radiation. Front. Plant Sci. 7, 1337.

McKenna, A., Hanna, M., Banks, E., Sivachenko, A., Cibulskis, K., Kernytsky, A., Garimella, K., Altshuler, D., Gabriel, S., Daly, M., DePristo, M.A., 2010. The genome analysis toolkit: a MapReduce framework for analyzing next-generation DNA sequencing data. Genome Res. 20, 1297–1303.

Mckenzie, R.L., Aucamp, P.J., Bais, A.F., BjāRn, L.O., Ilyas, M., Madronich, S., 2011. Ozone depletion and climate change: impacts on UV radiation. Photochem. Photobiol. Sci. 10, 182–198.

Moazzam-Jazi, M., Ghasemi, S., Seyedi, S.M., Niknam, V., 2018. COP1 plays a prominent role in drought stress tolerance in Arabidopsis and Pea. Plant Physiol. Biochem. 130, 678–691.

Núñez-Pons, L., Avila, C., Romano, G., Verde, C., Giordano, D., 2018. UV-protective compounds in marine organisms from the southern ocean. Mar. Drugs 16, 1–55.

Paul, N.D., Gwynn-Jones, D., 2003. Ecological roles of solar UV radiation: towards an integrated approach. Trends Ecol. Evol. 18, 48–55.

Pereira, B.K., Rosa, R.M., Silva, J., Guecheva, T.N., Oliveira, I.M., Ianistcki, M., Benvegnú, V.C., Furtado, G.V., Ferraz, A., Richter, M.F., Schroder, N., Pereira, A.B., Henriques, J.A., 2009. Protective effects of three extracts from Antarctic plants against ultraviolet radiation in several biological models. J. Photochem. Photobiol., B 96, 117–129.

Righini, S., Rodriguez, E.J., Berosich, C., Grotewold, E., Casati, P., Ferreyra, M.L.F., 2018. Apigenin produced by maize flavone synthase I and II protects plants against UV-B-induced damage. Plant Cell Environ. https://doi.org/10.1111/pce.13428.

Robinson, S.A., Erickson, D.J., 2015. Not just about sunburn–the ozone hole's profound effect on climate has significant implications for Southern Hemisphere ecosystems. Global Change Biol. 21, 515–527.

Rold-Anarjona, T., Ariza, R.R., 2009. Repair and tolerance of oxidative DNA damage in plants. Mutat. Res. 681, 169–179.

Shi, H., Ye, T., Chan, Z., 2014. Comparative proteomic responses of two bermudagrass (*Cynodon dactylon* (L).Pers.) varieties contrasting in drought stress resistance. Plant Physiol. Biochem. 82, 218–228.

Singh, J., Dubey, A.K., Singh, R.P., 2010. Antarctic terrestrial ecosystem and role of pigments in enhanced UV-B radiations. Rev. Environ. Sci. Biotechnol. 10, 63–77.

Singh, J., Singh, R.P., 2014. Adverse effects of UV-B radiation on plants growing at Schirmacher Oasis, East Antarctica. Toxicol. Int. 21, 101–106.

Takshak, S., Agrawal, S.B., 2015. Defence strategies adopted by the medicinal plant *Coleus forskohlii* against supplemental ultraviolet-B radiation: augmentation of secondary metabolites and antioxidants. Plant Physiol. Biochem. 97, 124–138.

Tamura, K., Peterson, D., Peterson, n., Stecher, G., nei, M., Kumar, S., 2011. MEGA5: molecular evolutionary genetics analysis using maximum likelihood, evolutionary distance, and maximum parsimony methods. Mol. Biol. Evol. 28, 2731–2739.

Tian, Y., Li, Y.L., Zhao, F.C., 2017. Secondary metabolites from polar organisms. Mar. Drugs 15, 1–30.

Tilbrook, K., Dubois, M., Crocco, C.D., Ruohe, Y., Richard, C., Guillaume, A., Emanuel, S.S., Michel, G.C., Roman, U., 2016. UV-B perception and acclimation in *Chlamydomonas reinhardtii*. Plant Cell 28, 966.

Tuteja, N., Singh, M.B., Misra, M.K., Bhalla, P.L., Tuteja, R., 2001. Molecular mechanisms of DNA damage and repair: progress in Plants. Crit. Rev. Biochem. Mol. 36, 337–397.

Ulm, R., Nagy, F., 2005. Signalling and gene regulation in response to ultraviolet light. Curr. Opin. Plant Biol. 8, 477–482.

Waterman, M.J., Nugraha, A.S., Hendra, R., Ball, G.E., Robinson, S.A., Keller, P.A., 2017. Antarctic Moss biflavonoids show high antioxidant and ultraviolet-screening activity. J. Nat. Prod. 80, 2224–2231.

Wolf, L., Rizzini, L., Stracke, R., Ulm, R., Rensing, S.A., 2010. The molecular and physiological responses of *Physcomitrella patens* to ultraviolet-B radiation. Plant Physiol. 153, 1123–1134.

Xu, L., Yang, P., Feng, Y., Xu, H., Cao, Y., Tang, Y., Yuan, S., Liu, X., Ming, J., 2017. Spatiotemporal transcriptome analysis provides insights into bicolor tepal development in *Lilium* "Tiny Padhye". Front. Plant Sci. 8, 398.

Yang, S.L., Zhang, X.N., Lu, G.L., Wang, C.R., Wang, R., 2015. Regulation of gibberellin on gene expressions related with the lignin biosynthesis in 'Wangkumbae' pear (*Pyrus pyrifolia Nakai*) fruit. Plant Growth Regul. 76, 127–134.